Structural evolution of Pt, Au, and Cu anodes by electrolysis up to contact glow discharge electrolysis in alkaline electrolytes

Evelyn Artmann, Pramod V. Menezes, Lukas Forschner, Mohamed M. Elnagar, Ludwig A. Kibler, Timo Jacob,* and Albert K. Engstfeld*

Institute of Electrochemistry, Ulm University, D-89081 Ulm, Germany

E-mail: timo.jacob@uni-ulm.de; albert.engstfeld@uni-ulm.de
Phone: +49 (0)731 25401. Fax: +49 (0)731 25409

Abstract

Applying a voltage to metal electrodes in contact with aqueous electrolytes results in the electrolysis of water at low voltages and plasma formation in the electrolyte at high voltages referred to as contact glow discharge electrolysis (CGDE). While several studies explore parameters that lead to changes in the *I–U* characteristics in this voltage range, little is known about the evolution of the structural properties of the electrodes. Here we study this aspect on materials essential to electrocatalysis, namely Pt, Au, and Cu. The stationary *I–U* characteristics are almost identical for all electrodes. Detailed structural characterization by optical microscopy, scanning electron microscopy, and electrochemical approaches reveal that Pt is stable during electrolysis and CGDE, while Au and Cu exhibit a voltage-dependent oxide formation. More importantly, oxides are reduced when the Au and Cu electrodes are kept in the electrolysis solution. We suspect that H_2O_2 (formed during electrolysis) is responsible for the oxide reduction. The reduced oxides (which are also accessible *via* electrochemical reduction) form a porous film, representing a possible new class of materials in energy storage and conversion studies.

Introduction

Applying a voltage to metal electrodes in contact with aqueous electrolytes is used to catalyze Faraday and non-Faraday reactions,[1–3] tailor surface properties of electrodes,[4–7] form nanoparticles[8,9] or alter the electrolyte composition,[1,7] as well as to ignite plasmas in solution.[1,10,11] Depending on the application, a detailed understanding of the parameters that limit the electrode stability is decisive to prevent material degradation or to adjust the formation of specific structures. The electrode stability is highly dependent on the applied voltage and the processes occurring at the electrode surface, which change dramatically when the voltage is increased significantly. Focusing on gas-evolving working electrodes, the phenomena that are expected to occur at the solid | liquid interface can be summarized as follows. For low voltages, water electrolysis is observed (referred to as normal electrolysis - NE). Increasing the voltage leads to violent bubble formation until the so-called breakdown voltage, where a gas film (sheath) forms around the electrode. At even higher voltages, the formation of a homogeneous plasma is observed within this sheath, which is called contact glow discharge electrolysis (CGDE).[1,10–12]

Since the discovery of CGDE in aqueous electrolytes by H. Kellog in 1950,[10] there have been

several reports describing the shape of current-voltage (I–U) curves from NE to CGDE, exploring the impact of electrode material, electrolyte, temperature, pH, composition, electrode geometry, etc.[1,9,11–16] The most noteworthy observation for the present work is that during CGDE, the products formed at the interface are more diverse than those known from NE. For example, regardless of electrode polarity, both H_2 and O_2 may be formed simultaneously during CGDE. More importantly, in anodic CGDE, in addition significant amounts of H_2O_2 are also produced.[11,12,17] The origin of the formation of the product cocktail is caused by non-Faraday processes, where H_2O molecules decompose into highly reactive short-lived radicals and ions during CGDE, which react one with another in the plasma phase or at the plasma | liquid interface.[1,12,18]

Less is known on the evolution of the structural properties of the electrode material with increasing voltage from the NE to the CGDE regime.[6] Instead, the structural properties for both limiting regions are usually studied separately, for different reasons which is illustrated by the following examples. For the NE region electrode stability is an important aspect in electrocatalysis. Stable electrodes during the reaction are desired since degradation of the catalyst often lowers the efficiency. Besides, anodizing electrodes in aqueous electrolytes is used to form oxide structures or to smooth or clean materials via electropolishing.[4,19] When negative voltages are applied, the electrodes can undergo cathodic corrosion.[8,20–22] This approach can produce nanoparticles, tune the surface crystallographic orientation for catalytic reactions or other applications.[8,20–22] Regarding the high-voltage regime, where plasmas can be generated in liquid, is a growing area of research, aiming at a fundamental understanding of plasma formation, its interaction with the solid electrode and electrolyte, and to explore new fields of application.[5–7,18,23] Plasmas in liquid can be used to distinctly tailor the (near-)surface electrode properties, *i.e.*, to form durable oxide coatings on materials of complex sizes *via* plasma electrolytic oxidation (PEO)[24–26] or to remove irregularities from the workpiece *via* plasma electrolytic polishing (PEP).[6,27] As with cathodic corrosion, the electrodes can also decompose into (multi-)metallic or oxidic nanoparticles.[7,9,23,28–33] Such particles can also be formed from metal ions present in the electrolyte during plasma electrolysis.[7,34] Finally, another interesting and yet emerging field is the wastewater treatment by plasmas,[7,23,35–37] where the stability of the prepared electrodes is detrimental to prevent any kind of metal contamination in the water. These examples and applications show the broad application of plasma treatment and the importance of having a clear picture of any kind of plasma-induced structure changes or formation processes. Overall, the examples also raise the questions if similar or other structures to those observed in the the NE and CGDE regime, are accessible in the voltage regime in between.

This is subject of this work, which aims at providing more detailed and systematic insights into possible changes in the structural properties of gas-evolving metal electrodes, covering the voltages range from NE to CGDE. Motivated by their importance in electrochemistry and electrocatalysis, we restrict our investigations to processes at poly-crystalline Pt,[38–42] Au[43–45] and Cu[46–48] wire anodes. While various studies have addressed the structure of these electrodes at low potentials (NE regime), much less is known about their behavior during CGDE.[7,9–11,31,32,49] In our study, the electrodes are investigated by controlled–potential electrolysis at a set of voltages ranging from the NE region up to 580 V in 0.01 M KOH electrolyte. The resulting I–U behaviour is discussed based on the structural properties investigated after the electrolysis. The topography and microscopic changes of the electrodes are imaged with an optical microscope and by scanning electron microscopy (SEM). For the oxide-forming metals Au and Cu, the amount of oxide formed during electrolysis is determined after the electrolysis from chronoamperometric measurements performed at potentials below the reduction potential of the respective oxides. We demonstrate, that independent from the applied voltage during electrolysis (50 to 580 V), the Au and Cu oxides also reduce when

kept in the electrolysis solution after the electrolysis. The effect of H_2O_2 on the oxide reduction is discussed. Finally, we demonstrate that the oxide reduction leads to the formation of highly porous nanostructures, determined from combined cyclic voltammetry and SEM experiments.

Results and Discussion

In the following, first the *I–U* behavior of the different investigated metals is discussed, followed by detailed analyses of their rather specific and divergent structural and electrochemical properties. The general observations for all systems are finally summarized in the conclusion. A detailed description of the experimental conditions is provided at the end of the manuscript and further details are provided in the supporting information (SI).

I–U characteristics

Figure 1 shows stationary *I–U* characteristics of Pt, Au, and Cu wire electrodes (immersed 10 mm, diameter 0.5 mm) recorded for 30 s electrolysis in 0.01 M KOH where the averaged current values for each voltage were obtained with freshly prepared electrodes. The chronoamperometric curves for the individual values are provided in Fig. S1. Longer electrolysis times were avoided to prevent significant changes in electrolyte temperature, which can change the *I–U* behaviour significantly. For a similar reason, applying voltages above 580 V was avoided, where in addition the wire can easily melt. Details on the experimental approach, chronoamperometric measurements, data evaluation, and the effect of temperature are provided in the experimental section and the supporting information (Figs. S1 and S2).

The *I–U* behavior in Fig. 1 is characteristic for gas–evolving electrodes.[11,15,50] In the NE region up to the breakdown voltage (V_B) at ca. 350 V, the current increases linearly due to the limited conductivity of the electrolyte according to Ohms law. At V_B the resistance increases due to gas film formation around the electrode, which leads to a break down of the NE concomitant with a decrease in current density. The effect becomes more pronounced with increasing voltage. Close to the midpoint voltage (V_D) sparks are observed by visual inspection in the gas film forming around the electrode. At V_D the electrode is completely wrapped in a gas sheath and a blue-violet fast fluctuating plasma with an electrifying, sharply hissing sound is observed within the sheath.

Overall, the *I–U* characteristics are very similar for all three electrode materials investigated, and the current densities at the characteristic voltages V_B and V_D are almost identical. This suggests that for a given electrolyte the *I–U* behaviour is almost independent of the examined electrode material and that the material properties (i) do not change, (ii) change in a similar fashion, or (iii) changes of the material properties are not important for the *I–U* curves.

A direct comparison of the current values at specific voltages, specifically the occurrence of characteristic voltages (V_B and V_D), with results from literature is, however, not straightforward. As mentioned above, in general the *I–U* behavior strongly depends on the experimental conditions, and furthermore the values of the characteristic voltages strongly depend on the cell and electrode geometry.[1,9,11–16,51] Nevertheless, Hickling and Ingram investigated the *I–U* behavior of Pt, Au and Cu wire electrodes (among others), although in another electrolyte (0.05 M Na_2HP0_4). Their results showed that Au, Pd, and Pt show a very similar behavior during electrolysis at various voltages compared to W, Cu, or NiCr.[11] The authors suggested that on the latter metals oxide film formation and corrosion are at the origin of the different behavior compared to Au, Pd an Pt.[11] Our own results on the structural properties of the electrodes discussed below, will show that oxide formation occurs on Au and Cu electrodes. The fact that the *I–U* curves of Au and Cu are almost identical to that of Pt, suggests that the electron transport through the oxide film on Au and Cu is equally fast as for bare Pt electrodes.

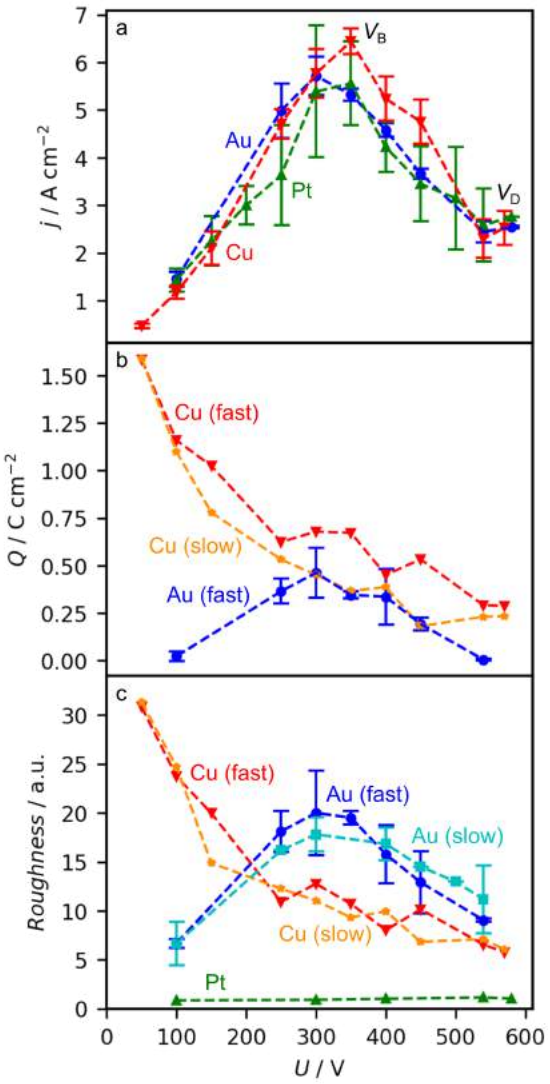

Figure 1: a) I–U characteristics, where each data point was recorded with a freshly prepared electrode for 30 s electrolysis in 0.01 M KOH. b) Cathodic charge density determined from the chronoamperometry measurements in Fig. 7 for Au, and for Cu, respectively, recorded after the electrolysis and subsequent electrochemical reduction. It is important to distinguish whether the electrode is removed immediately after the electrolysis from the solution (fast) or kept in the electrolysis solution for additional 60 s (slow). c) Change in roughness factor (RF) with respect to the as-prepared samples after the anodic polarization and subsequent electrochemical reduction determined from the CVs presented in Fig. 7 for Au, and Fig. 11 for Cu.

Structure formation

Further insights on the impact of the electrolysis on the structural properties of the electrodes is gained from optical microscopy, SEM, and detailed voltammetric studies of the electrodes, by comparing the data recorded before and after electrolysis. While the microscope images (optical and SEM) provide insights into the three-dimensional structural changes, from the cyclic voltammetry measurements we can additionally deduce (i) the amount of oxide formed during electrolysis, (ii) determine possible changes in the crystallographic orientation of the surface, and (iii) derive changes in surface area.[52,53] In the following, the electrode materials are discussed separately since the structural modifications of the investigated metals differ strongly one from another.

Pt

The SEM images of an as-prepared Pt wire and that after the electrolysis at 300 V for 30 s in 0.01 M KOH are depicted in Fig. 2. Further images obtained for other electrolysis voltages (100 and 580 V) are provided in Fig. S3. The SEM images suggest that the Pt surface does not restructure significantly during electrolysis at any applied voltage.

To substantiate this finding, we studied the electrodes by cyclic voltammetry. The cyclic voltammograms (CVs) recorded for the Pt electrodes in 0.01 M KOH at 50 mV s^{-1} before (black) and after electrolysis (blue & orange) are presented in Fig. 3. All potentials in the electrochemical experiments are on the reversible hydrogen electrode (RHE) scale unless otherwise mentioned. The CVs show the typical features for hydrogen ad-/desorption (between 0.05 and 0.55 V) and OH/O ad-/desorption (between 0.7 and 1.0 or 1.5 V) on Pt in alkaline electrolytes.[54] The downshift of the current in the hydrogen region is caused by residual oxygen in the cell. For the first voltammetric cycle recorded after the electrolysis (blue), the upper potential limit was fixed at 1.0 V to avoid significant surface restructuring which would occur by applying higher potentials.[55–58] The CV recorded with an upper

potential limit of 1.45 V (orange) was subsequently recorded.

The peaks in the CV are located at almost the same potentials, and also the current densities at the peak maxima are rather similar, hence the crystallographic orientation of the surface did not change measurably. The small changes in the current density are within the limits of the experimental precision. This may be because the immersion depth of the wires cannot always be set precisely the same. Nevertheless, the almost similar current densities in CVs recorded before and after the electrolysis suggest that the surface area does not change significantly. Henceforth the change in electrochemical surface area is denoted as roughness factor (RF), which is described in detail in the experimental section. For Pt the RF remains almost at unity, as shown in Fig. 1 c (green triangles). Note that much more sensitive methods are needed to resolve possible restructuring processes on the atomic scale. For the high voltage region (CGDE), Pt was previously suggested to be stable in a wide range of electrolytes.[10,11,13,59–61] This is different in the NE region, where surface restructuring would have been expected from the work by Favaro *et al.* Studying the oxygen evolution reaction (OER) on Pt electrodes in alkaline electrolytes, they observed a restructuring of the electrodes with *ex situ* atomic force microscopy (AFM) after the OER. They also observed the formation of a complex, several nm thick oxy-hydroxy film forms on the electrode surface, elucidated by using ambient pressure X-ray photoelectron spectroscopy (APXPS). Bulk oxide formation under these conditions was also suggested by theoretical studies to be thermodynamically favorable at high overpotentials for Pt nanoparticles.[62]

From studying the first negative potential scan of the CV starting from 0.95 V in our experiment, we did not observe any currents related to oxide reduction. Even thought we cannot completely rule out that the surfaces reduce during the transfer from one electrochemical cell to another, based on our results we suggest that oxide formation might not occur during electrolysis at voltages above 100 V in alkaline electrolyte.

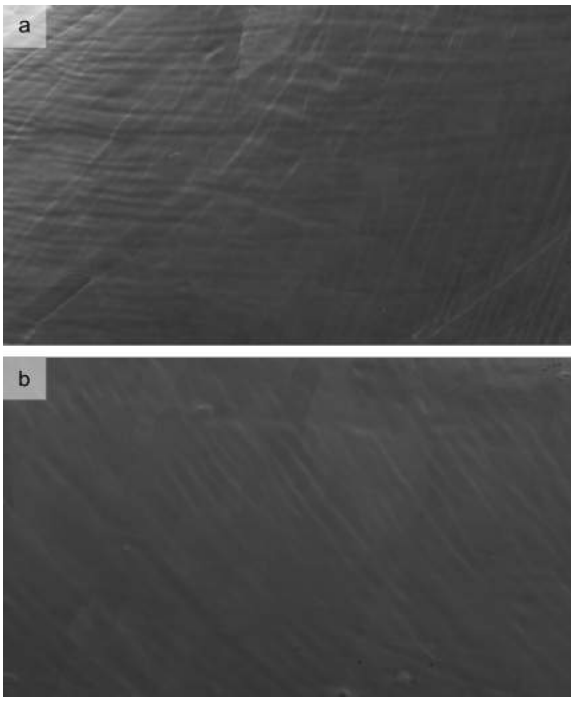

Figure 2: SEM images (250 μm $\times$ 150 μm) of a Pt wire electrode a) as-prepared and b) after electrolysis at 300 V for 30 s in 0.01 M KOH. Further SEM images are provided in Fig. S3.

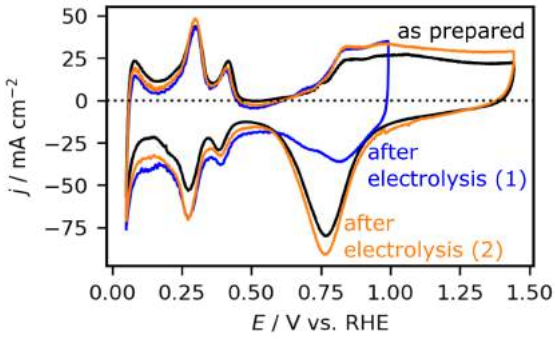

Figure 3: CVs recorded in 0.01 M KOH at 50 mV s^{-1} of an as-prepared Pt electrode (black curve) and the same electrode after the electrolysis at 300 V for 30 s in 0.01 M KOH. The first CV after the electrolysis was recorded with an upper potential limit of 1.0 V (blue). Subsequently, additional cycles were recorded with an upper potential limit of 1.45 V (orange).

Au

After performing electrolysis at different voltages for 30 s in 0.01 M KOH (as in Fig. 1 a), inspection of the Au electrodes by the naked eye revealed a color change for all voltages. In addition, the intensity and color depends on the applied voltage and more importantly on the time of exposure of the electrode to the electrolyte after the electrolysis. This is demonstrated by the optical microscope image in Fig. 4 for a Au electrode on which 300 V were applied during electrolysis. If the electrode is immediately removed from the electrolyte after electrolysis the electrode is mostly red (Region 1), whereas the electrode part that was kept in the electrolysis solution turns black within a few seconds (Region 3). Respective microscope images taken after the electrolysis at different voltages are provided in Figs. 5 a to d (first column) along with selected SEM images recorded on the red region (1), transition region (2), and black region (3) in the second to the fourth column. Overall, the red color of the Au wire suggests that a Au_2O_3 layer is formed during the electrolysis on the electrode.

Focusing on the red part (region 1), obtained by electrolysis and subsequently direct removal of the electrode from the electrolyte solution, we observe in the optical microscope images that the intensity of the red color varies with the applied voltage. At 300 and 400 V the red tone is rather intense, while at 100 and 540 V the red color is less pronounced and shows a touch of orange. Corresponding SEM images are provided in Figs. 5 e to h (second column). For all voltages, the surface shows large flat regions and several approximately 150 nm wide cracks. In some regions it seems as if the newly formed adlayer peels off from the Au wire substrate. While the origin of this process is unclear, we suggest that this can be caused by the emersion and immersion of the electrode during the transfer between the different electrochemical cells. The holes observed in the SEM images, especially in Figs. 5 e to g, are primarily induced by the electron beam of the SEM (see Fig. S4).

The amount of oxide formed during electrolysis was quantified by electrochemical reduction in 0.01 M KOH, as shown in Fig. 6. Here the potential was swept at 50 mV s^{-1} from an initial potential of 1.10 V to 0.25 V, where the potential was kept until the reduction current became insignificant (up to 50 s). The total charge passed during these chronoamperometry measurements is depicted in Fig. 1 b. The trend in charge density passed follows the *I–U* behaviour in Fig. 1 a, where the largest charge density is obtained for electrolysis at 300 V. For voltages around 100 V and 540 V the oxide formation is not significant. Considering that the charge density is related to the amount of oxide formed per cm^2, during 30 s of electrolysis the thickest oxide film is formed at around 300 V. Another important observation is that the initially red electrode turned black during the reduction process. SEM imaging of these reduced electrodes revealed a highly porous structure which is depicted in Fig. S5. Such a change in color has been reported recently for the reduction of Au_2O_3 to metallic Au,[63] and the black color has been attributed to the ability of the nanostructured Au surface to absorb significantly the incident light from the visible spectrum.[64,65]

Comparing the CV of an as-prepared Au wire electrode (Fig. 7 a) with those obtained after the electrolysis and subsequent electrochemical reduction in Fig. 7 b, overall higher current densities are observed for the latter electrodes. Note that all current densities are normalized to the initial geometric surface area of the wire. No additional peaks or changes in relative peak sizes are observed in the CVs, which would indicate a change of surface structure or crystallographic orientation.[21,22] The shift of the oxidation (reduction) peaks to more positive (negative) potentials for higher current densities is presumably caused by internal resistance effects. The increase in Faraday current suggests a strong increase in surface area, especially for electrolysis at around 300 V, which is apparent from the change in RF shown in Fig. 1 c (labeled Au fast). The evolution of the RF after reduction of the Au_2O_3 phase formed during the electrolysis with increasing voltage follows the overall trend of the *I–U* and *Q-U* curves

Figure 4: Microscope image of a Au wire after electrolysis at 300 V for 30 s in 0.01 M KOH. The left (golden) part shows the as-prepared Au wire, the middle (red) part (region 1) was immediately removed from the electrolyte after the electrolysis, and the right (black) part (region 3) was kept in the electrolysis solution for 60 s after switching the voltage off. Region 2 marks the transition between regions 1 and 3.

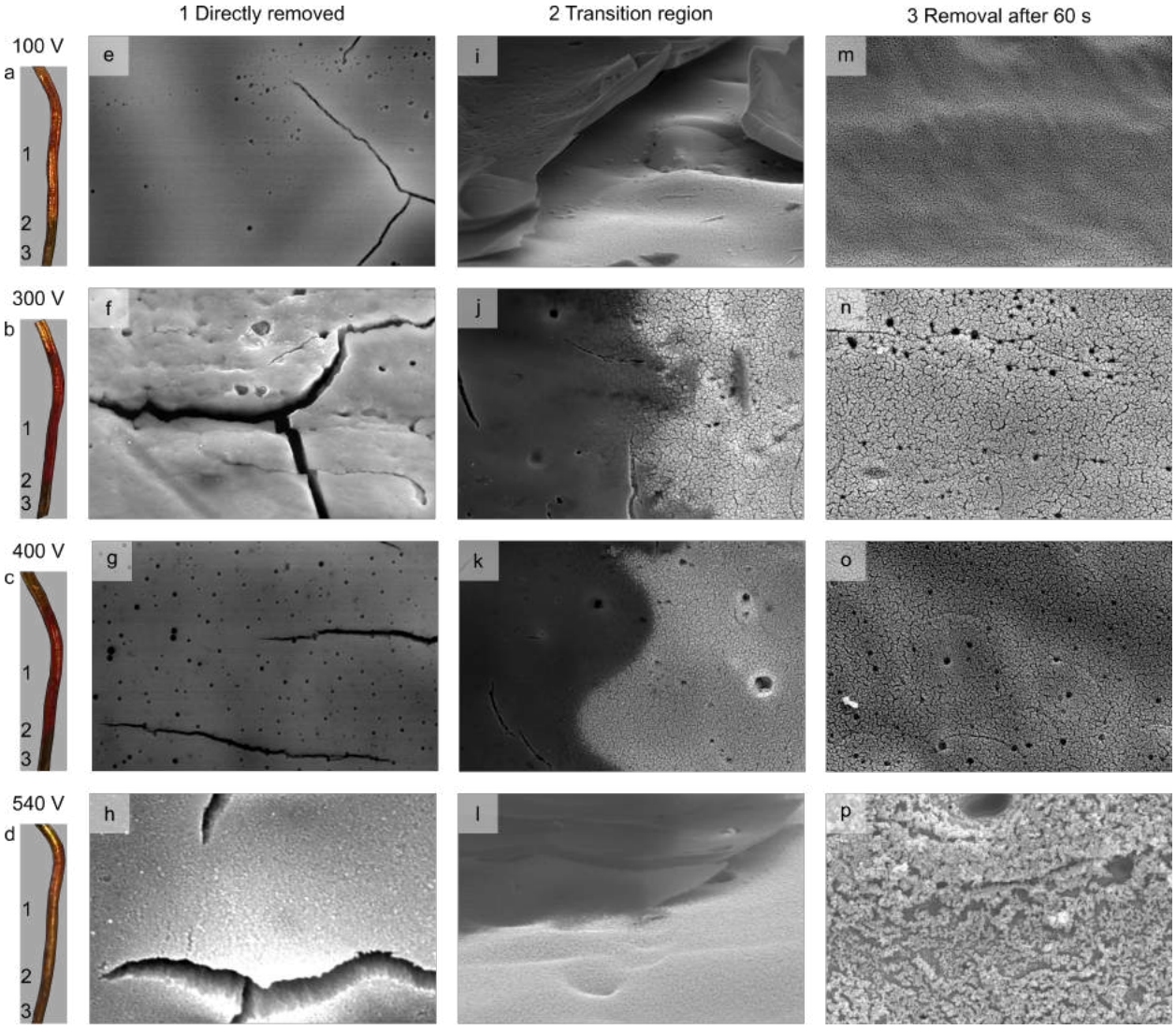

Figure 5: Left column: Optical microscope images of Au wires taken after electrolysis at the given voltages for 30 s in 0.01 M KOH. The numbers in the optical microscope images (a-d) illustrate the different regions in Fig. 4. The second to fourth column show from left to right SEM images of the regions 1-3 (12 μm $\times$ 8 μm), recorded after electrolysis at different voltages.

of Figs. 1 a and b, where the highest RF value is obtained at V_B (ca. 300 V). Interestingly, for electrolysis at 100 and 540 V, where the amount of surface oxide was low (Fig. 1 b), the increase in surface area is still significant but lower than at V_B. Possible reasons for the voltage-dependent growth rates are yet to be resolved.

A peculiar observation is that the Au electrodes also turn black when they are kept in the electrolysis solution for 60 s after the electrolysis (see region 3 in Fig. 4). Unlike for the red part (region 1), the intensity of the color is similar for all voltages. Corresponding SEM images are provided in Figs. 5 m to p (fourth column). Compared to the red part of the electrode, the surface is much more porous, with a sponge-like surface structure that looks very similar to that obtained after the electrochemical reduction of the Au_2O_3 above. For a better comparison between the structures, in Figs. 5 i to l (third column) we depict the transition region (region 2) between the red and black parts. In these images, the red Au_2O_3 region appears darker than the black nanoporous metallic Au region.

Inspection of the black region by cyclic voltammetry did not show any signs of surface or near-surface oxide reduction in the first negative-going scan in contrast to the red part of the Au wire. Instead, the CVs look almost identical to those obtained after electrochemical reduction of the red electrodes shown in Fig. 7 b, and also the RF is almost identical to those obtained for the red electrodes polarized at similar voltages (Fig. 1 c – labelled Au slow).

To elucidate the origin of the color change of the Au electrodes kept in the electrolysis solution, we first stored electrodes directly removed from the electrolysis solution under ambient conditions or in a fresh 0.01 M KOH solution for 24 to 48 hours. This did not induce a color change, and hence, the structural change had to be caused by species present in the solution after electrolysis. For low voltages (NE), it is expected that mainly O_2 is formed from water splitting. At significantly high voltages, in the region of CGDE (in our case $> 540\ V$), it has been demonstrated that after the electrolysis in addition to O_2, also H_2 or H_2O_2 were detected.[11,17,59] In a further set of experiments, the Au electrodes that were removed immediately after electrolysis were dipped into KOH solutions saturated with H_2, O_2, or mixed with H_2O_2. We could only observe a color change from red to black in the H_2O_2 containing solution, hence it is reasonable to assume that the H_2O_2 is at the origin of the reduction process at least at high voltages. To what extent highly-reactive, short-living or excited radicals and ions, present during and shortly after CGDE, contribute to the reduction process after the electrolysis can not be deduced from our experiment. The origin of the oxide reduction at lower voltages in the electrolyis solution can only be speculated on, and further experiments are required to elucidate whether H_2O_2 possibly forms under these experimental conditions.

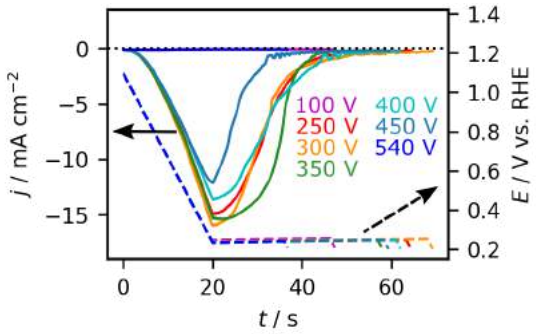

Figure 6: Characterization of the amount of oxide formed on Au wires after electrolysis in 0.01 M KOH at the given voltages. The potential was swept at 50 mV $s^{-1}$from the initial potential of 1.1 V to 0.25 V, where the potential was held until the reductive current became insignificant.

Cu

As in the case of Au, for Cu electrodes also the the impact of removing the electrodes immediately after the electrolysis from the electrolyte and after keeping the electrodes for additional 60 s in the electrolysis solution was investigated. Independent of the experimental procedure, the Cu electrodes turned black. Only with the optical microscope subtle color changes are observed on a wire treated by both approaches,

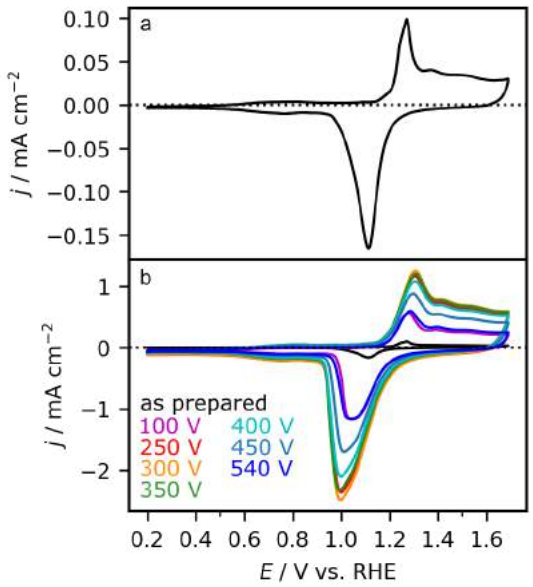

Figure 7: CVs of a) an as prepared Au wire (black) and b) the same electrode in comparison to the electrochemically reduced electrodes in Fig. 6 (previously treated by electrolysis at the given voltages). The CVs were recorded at 50 mV s^{-1} in 0.01 M KOH.

as shown in Fig. 8. The color changes were independent of the applied voltage during electrolysis. The black color strongly implies that a Cu(II)-oxide (CuO) is formed. Note that Cu(I)-oxide (Cu_2O) is red. The origin of the two black regions is discussed below.

Figure 9 shows SEM images taken on regions of the Cu wires removed directly after the electrolysis (left column) and kept in the solution for additional 60 s (center column). In the supporting information, Fig. S6 shows additional SEM images depicting a larger surface area. The SEM images do not suggest distinct structural differences between both experimental approaches, even though both regions show slightly different colors in the optical microscope (Fig. 8). Hence, the following description applies to both regions 1 and 3 depicted in Fig. 8. In contrast to Pt and Au, the SEM images of Cu (Fig. 9) demonstrate macroscopic surface structural changes as a function of the applied voltages. After electrolysis at low voltages (until 100 V), 3D flake-like structures are formed. Three-dimensional macroscopic structure formation for Cu electrodes in alkaline media is not uncommon.[66–68] Performing electrolysis at intermediate voltages (250 V) results in pitting of the surface. Performing electrolysis at high voltages, including the region for CGDE, the surface becomes more smooth.

As indicated above, the color change of the electrode during the electrolysis to black strongly implies that a CuO is formed. To quantify the amount of oxide, the electrodes were electrochemically reduced in 0.1 M KOH by sweeping the potential at 50 mV s^{-1} from 0.31 V to a potential beyond -0.2 V and kept at a potential lower than -0.2 V until the reduction current becomes insignificant (up to 40 s), as shown in Fig. 10. In principle, it is possible to determine the type of Cu oxide or hydroxide from the peak position in the negative-going scan direction of the CV.[68] However, in this case (see Fig. 6) the amount of oxide is rather high such that distinct well-separated reduction peaks could not be resolved and the contribution from the reduction of different Cu oxides/hydroxides overlap. Nevertheless, based on the work by Deng and coworkers, who studied the OER in alkaline electrolyte, identified CuO along with $Cu^{III}O_2^-$ compounds by XANES and *in situ* Raman spectroscopy.[68] In combination with K^+ or Na^+, such cuprates have a bluish-black color. From visual inspection, these compounds cannot be discerned. Electrochemically, it was suggested that the Cu(III) compounds could be reduced at potentials below 1.6 V and can be identified by a peak at potentials slightly below 1.6 V.[68] With our experimental approach, it is, however, not possible to identify the Cu(III) compounds since our starting potential (0.31 V) in the chronoamperometry measurements in Fig. 10 is already below 1.6 V. Nevertheless, it is very likely that both Cu(II) and Cu(III) compounds form during the electrolysis at high voltages. Additional experiments are, however, required to confirm this assumption and elucidate the nature of the surface oxides formed.

In contrast to Au, independent of the pretreatment, *i.e.*, direct removal of the electrodes after the electrolysis (Cu fast) or keeping the electrode in the electrolysis solution (Cu slow), a reduction current is measured on all Cu

Figure 8: Microscope image of a Cu wire after electrolysis at 300 V for 30 s in 0.01 M KOH. The left part of the microscope image shows the as-prepared Cu wire. Region 1 shows the part of the wire which was immediately removed from the electrolyte after the electrolysis, where region 3 was obtained from keeping the electrode in the electrolyte for 60 s. Region 2 is the transition between region 1 and 3. The contrast and brightness of the image was visually improved for better visibility of the two regions.

electrodes. The corresponding charge density passed during the electrochemical reduction of the electrodes (Fig. 10) is depicted in Fig. 1 b for all investigated electrodes, along with the data obtained for Pt and Au. Overall, the charge density decreases almost exponentially with increasing applied voltage. In comparison to Au, the oxide formation is also still significant during CGDE.

For almost all electrolysis voltages in Fig. 1 c, it is apparent that the charge densities passed for the electrodes removed immediately after the electrolysis (Cu fast - red) are larger than those kept in the electrolysis solution (Cu slow - orange). Hence the electrodes are partially reduced when they are kept in the solution after electrolysis. Similar to the case of Au discussed above, we suggest that species in the electrolysis solution formed during the electrolysis, *i.e.*, H_2O_2, cause the reduction. Considering that Cu(III) compounds are formed during electrolysis (see above) and that these compounds are reduced at more positive potentials than the oxides that are reduced in the potential window of our electrochemical reduction experiment in Fig. 10, we suggest that Cu(III) compounds are reduced to Cu(II) compounds under these conditions. Since the difference in charge density is small for both experimental procedures, it further implies that the amount of Cu(III) compounds formed during electrolysis is comparatively low.

The structural changes induced by the electrolysis and subsequent electrochemical reduction of the electrodes were investigated by cyclic voltammetry. The CV of an as-prepared electrode is shown in Fig. 11 a and b (black), and these recorded after the electrolysis at 50, 300, and 570 V are shown in Fig. 11 b. In the latter, we also differentiate between electrodes, which were removed immediately from the electrolysis solution (solid lines), and those which were kept for additional 60 s in the electrolyte (dash-dotted lines). In general, for Cu electrodes the peaks at potentials larger than 0.2 V can be attributed to the formation and reduction of Cu_2O. The peaks at potentials smaller than 0.2 V can be attributed to surface OH adsorption and desorption on different low index surfaces.[69–72] From the comparison of the CVs of the as-prepared electrode with those recorded after electrolysis and subsequent reduction, it is apparent that the voltammetric features in the CV change, indicating that the crystallographic orientation of the electrode surface changed.[69] Interestingly, the characteristic features of the voltammograms recorded after electrolysis at different voltages are very similar for all electrodes, indicating that all electrodes have a similar surface crystallographic orientation. In addition, the RF of Cu increased in comparison to the as-prepared Cu electrodes shown in Fig. 1 c and is independent from the experimental procedure (immediate removal of the electrode after electrolysis or keeping the electrode in the electrolysis solution).

In turn, the RF decreases exponentially from 50 to 570 V, following the voltage-dependent evolution of the charge density. Note that for electrolysis in the CGDE region, the electrodes still have a six times larger surface area than the as-prepared Cu wire. The change in surface

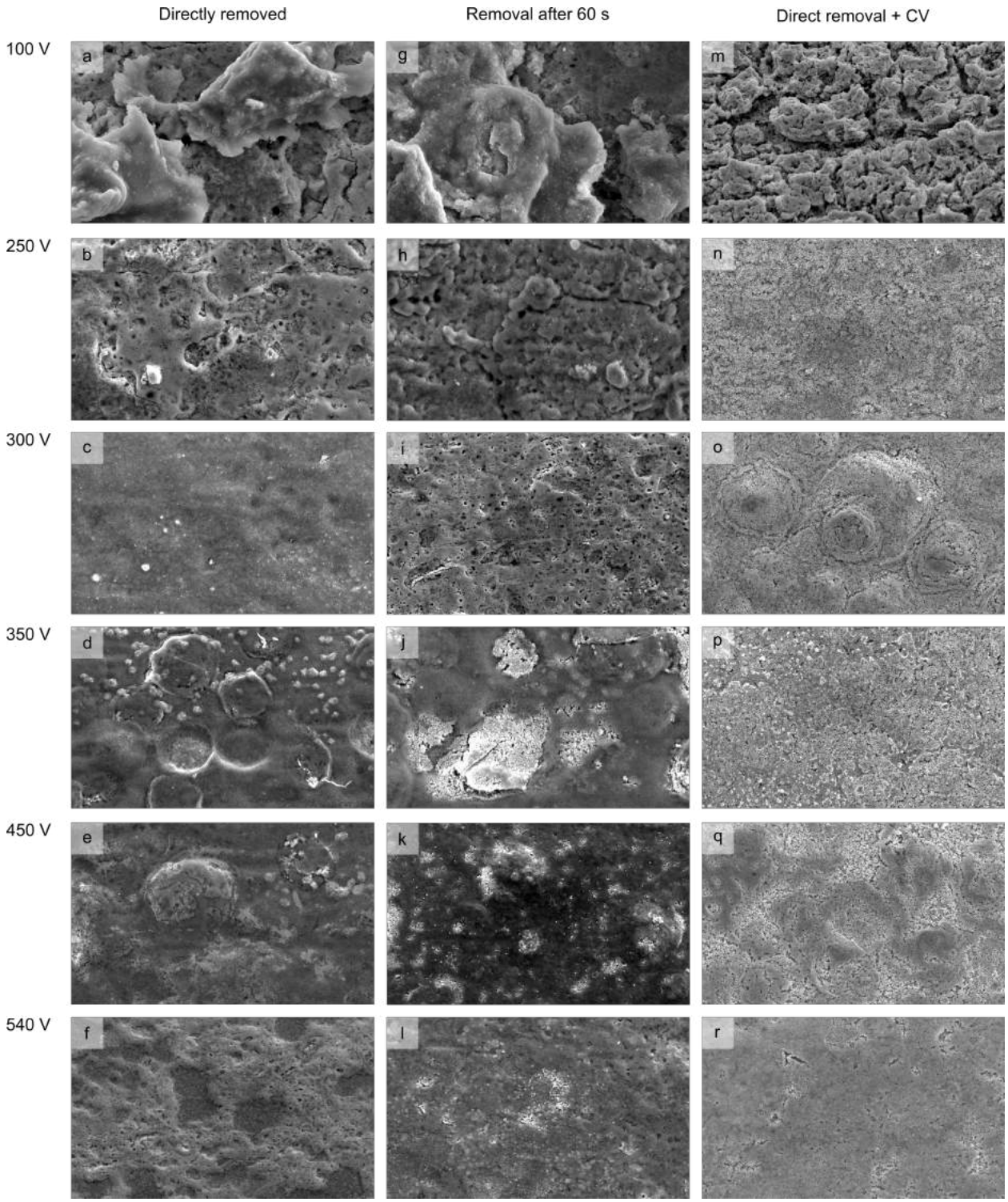

Figure 9: SEM images (50 μm $\times$ 30 μm) of Cu wire electrodes (length: 10 mm, diameter: 0.5 mm) after the electrolysis at the given voltages for 30 s in 0.01 M KOH. The first column (a-f) shows micrographs of the surface structures of the wires that were directly removed after the electrolysis, the second column (g-l) after keeping them in the electrolysis solution for 60 s , and the third column (m-r) after direct removal of the wires and subsequent electrochemical characterization.

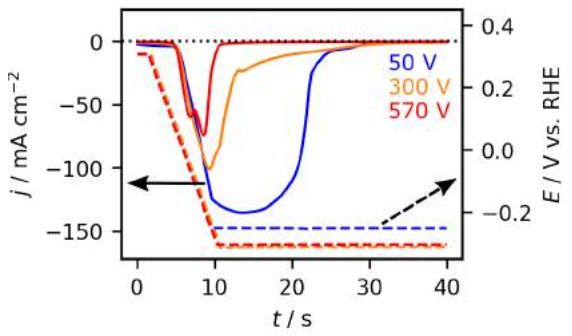

Figure 10: Characterization of the amount of oxide formed on Cu electrodes after the electrolysis at the given voltages, by sweeping the potential from 0.31 V to a potential beyond -0.2 V until the reductive current almost vanished.

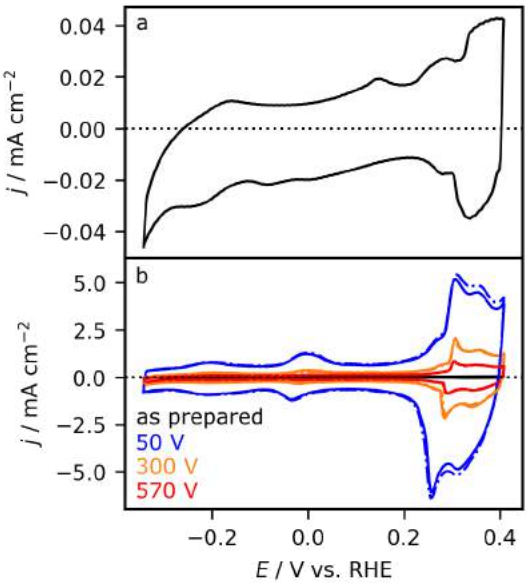

Figure 11: CVs of a) an as-prepared Cu wire (black) and b) the same electrode in comparison to the electrochemically reduced electrodes in Fig. 10 (previously treated by electrolysis at the given voltages). The CVs were recorded at 50 mV s^{-1} in 0.01 M KOH. The CVs presented in b) with solid lines were measured after direct removal of the electrodes from the electrolysis solution and subsequent electrochemical reduction in Fig. 10. In contrast, the CVs in dashed-dotted lines were recorded after keeping the electrodes in the electrolysis solution for 60 s and subsequent complete electrochemical reduction (reduction data not shown).

area is, to some extent, also apparent in the SEM images in Fig. 9 m to r (right column), where the surfaces became smoother with increasing voltage. Comparing the SEM images taken directly after the electrolysis (Fig. 9 g to l - middle column) with those taken after the electrochemical reduction (Fig. 9 m to r - right column), shows that the more rough surfaces obtained after electrolysis at low voltages stay rough after the electrolysis (compare images in Figs. 9 a, g, m – first row). In a similar way the more flat surfaces obtained at high voltages also remain mostly flat after the electrochemical reduction (compare images in Figs. 9 f, l, r – last row). Furthermore, SEM images taken at higher magnification in Fig. S7 show, the formation of a porous structure after the electrochemical reduction. Overall, the structure formation of Cu is very similar to that observed for Au above, except that the oxide layer thickness and the porosity of the film shows a different voltage dependence.

Summary and Conclusions

In this work, we investigated the impact of electrolysis on the structural properties of Pt, Au, and Cu electrodes in a 0.01 M KOH solution in a voltage range from 50 to 580 V. We show that the *I*–*U* characteristics are rather independent of the metal employed. Nevertheless, additional optical microscope, SEM, and electrochemical measurements clearly demonstrate that the structural properties differ strongly after the electrolysis. The following key observations were made, and questions remain:

1. Pt seems to be stable during electrolysis in agreement with previous studies in different electrolytes. Possible restructuring of the electrode on an atomic scale level or dissolution of the electrode could not be observed.

2. During electrolysis, an oxide film is formed on the Au and Cu electrodes, where the rate of formation depends on the metal and the applied voltage. The red color of the Au wire suggests that

Au_2O_3 is formed. In SEM images, the film appears rather flat and based on the charge density passed during the electrochemical reduction of the electrodes the oxide is thickest after electrolysis at the breakdown voltage of normal electrolysis (300 V). The black color of the Cu wire suggests that CuO is formed, which is rather textured (rough) and thickest for low voltages (50 V) and more flat and thinner in the CGDE region (540 V). Possible Cu(III) oxide formation, which was suggested to occur in the OER region under alkaline conditions, is very likely.[68] Further XPS measurements would be required to elucidate the oxidation state of the respective metals.

3. When the Au and Cu electrodes are kept for 30 s after the electrolysis in the electrolysis solution, their color changed from red to black for Au and from black to light black for Cu. Further electrochemical reduction measurements revealed that the Au oxide was completely and Cu oxide only partly reduced in the electrolysis solution. In the case of Cu we suggest that the partial reduction is attributed to the reduction of Cu(III) compounds. The content of which is low and less stable than CuO or Cu_2O.[68] Our preliminary results to explain the reduction process on Au_2O_3 suggest that H_2O_2, present in the electrolysis solution after the electrolysis, is at the origin of the oxide reduction. While it is known that H_2O_2 is formed during CGDE,[11,17] the formation at lower voltages has so far not been considered.

4. Reducing the oxides formed during electrolysis, either by keeping the electrodes in the electrolysis solution (for Au) or reducing the oxide electrochemically (for Au and Cu), leads to the formation of a high surface area nanoporous film. The change in electrochemical surface area to the as-prepared electrodes follows the same trend as the charge density determined from the reduction experiments. In the case of Au, the final porous structure is also independent of the reduction procedure.

Overall, performing electrolysis at high voltages on Au and Cu can be used to form thick oxide layers on the electrodes. Based on our findings, the oxide structure and film thickness differ significantly for the different metals, and the oxide structure also depends on the applied voltage. Similarly, the surface area of the porous films depends on the applied voltage during electrolysis. Hence, if this approach were used to prepare oxide or porous films with specific film thickness on other metals, a systematic study of the whole voltage range is inevitable. Reasons for the voltage-dependent oxide growth rates still have to be elucidated. Note that it is also mandatory to remove the electrodes swiftly from the electrolysis solution to assess properly the surface structures formed during electrolysis. Finally, such oxide-covered or highly-restructured materials with high surface area obtained from an initial electrolysis treatment could provide a new class of materials for possible applications as model electrodes in electrocatalysis, battery- and other energy-related research fields.

Experimental Section

Materials: All aqueous solutions were prepared by mixing Milli-Q water (18.2 MΩ cm, TOC $\leq$ 3 ppb) with KOH pellets (99.99 %, Sigma-Aldrich), 30 % HCl (Merck, Suprapur) or 85 % phosphoric acid (Merck, Suprapur).

Wires of Pt, Au, and Cu with a diameter of 0.5 mm were purchased from MaTecK (purity at least 99.99 %).

Sample preparation: In the case of Pt and Au, the same electrodes were used for all experiments, which were freshly prepared for each measurement. Both electrodes were flame annealed for three minutes in a Propane flame (MTI). In some cases, when the Au wire was strongly restructured during the electrolysis experiment, it was electropolished in 1 M HCl solution (10 V vs. a graphite CE) and subsequently annealed for a further three minutes in

the Propane flame.

In the case of Cu, a new wire was freshly prepared for each measurement. The Cu wires were sonicated in 85% phosphoric acid for one minute at room temperature to remove the native surface oxide layer. Subsequently, the Cu wires were thoroughly rinsed with MilliQ water and dried in air.

Electrolysis and electrochemical characterization: The electrolysis experiments (NE and aCGDE) and the electrochemical characterization were performed in separate electrochemical cells. This was necessary since usually during the electrolysis, the electrolyte properties change, *i.e.*, temperature, dissolved products such as H_2, O_2, and H_2O_2, which can affect the electrochemical characterization. All experiments were performed without stirring the electrolyte.

The electrolysis was performed in a glass cell containing 60 mL of 0.01 M KOH. A stainless steel plate of 15 mm × 20 mm × 3.5 mm was used as a counter electrode. The Pt and Au working electrode wires were immersed 10 mm into the electrolyte solution (4.5 or 10 mm for Cu) and was placed 2.5 cm apart from the counter electrode. The voltage for the electrolysis was applied for all electrodes for 30 s with a TDK-Lambda Power Supply (630 V / 1.365 A) controlled *via* a LabVIEW software. Each electrolysis experiment was performed in a fresh electrolyte. The anode wire was either prepared again (Pt and Au), or a new electrode was used (Cu) to guarantee identical conditions for each experiment. For the presentation of the *I–U* plot in Fig. 1, the data points were averaged for the 30 s electrolysis. The current density was determined from the geometric area of the wire electrode. During the 30 s electrolysis, the electrolyte temperature increases, leading to changes in the current density. Corresponding chronoamperometric curves are given in Fig. S1 along with a more detailed description of the temperature effects. The measurements were repeated several times, and the values were averaged afterward. The error bars are derived from several experiments performed under similar conditions.

The electrochemical characterization of Pt and Au was performed in a glass beaker cell containing 150 mL of 0.01 M KOH. A homemade reversible hydrogen electrode (RHE) was used as a reference electrode and a Pt-sheet (10 × 7.5 mm) as a counter electrode. All potentials are given on the RHE scale unless otherwise mentioned. The potential was controlled with a FHI ELAB potentiostat. The electrochemical properties for Pt and Au electrodes were investigated before and after the electrolysis.

The initial scan direction in the CV was negative for Pt, starting from 0.95 V (close to the open circuit potential). Before the electrolysis, the potential window of the cyclic voltammogram (CV) was fixed between 0.05 and 1.45 V. After electrolysis, first several cycles were recorded between 0.05 and 1.0 V to avoid significant surface restructuring. Subsequently, additional cycles with an upper potential limit of 1.45 V were recorded for comparison with the last CV recorded before the electrolysis.

The initial scan direction was negative for Au, starting from 1.1 V. The CVs were recorded in a potential window of 0.20 to 1.69 V. After the electrolysis, the surface was reduced electrochemically by holding the potential at 0.25 V in the first negative scan until the reduction currents became insignificant. The resulting charge densities are discussed in the manuscript.

For Cu, the electrochemical characterization was performed in a conventional three-electrode glass cell in 0.1 M KOH with a Hg/HgO reference electrode (RE-61AP, ALS) and a graphite rod as a counter electrode. The potential was controlled with a HEKA PG510 potentiostat. The starting potential to record the Cu CVs was 0.31 V, and the potential window was -0.34 V to 0.41 V. The characterization by cyclic voltammetry before the electrolysis was only performed on a few samples to ensure that the preparation procedure yielded reproducible CVs and hence similar surface structures. After the electrolysis, the surface oxide was reduced by holding the electrode at potentials < -0.2 V until the currents related to oxide reduction

became insignificant.

Surface area: All current densities are related to the original geometric surface area (Pt, Au: 0.16 cm^2, Cu: 0.07 or 0.16 cm^2) of the electrodes, determined from the wire length and diameter.

Charge density: The oxide formed on Au and Cu during electrolysis was reduced by scanning at 50 mV s^{-1} from the starting potential of the CV (see above)to the lower potential limit and keeping the electrode at that potential until the reduction currents disappeared. The charge density is obatained from integrating the current density, which in turn corresponds to the amount of oxide formed on the electrode. Note that a small fraction of the charge density is possibly also related to the reduction of residual molecular oxygen in the electrolyte. These currents are, however, small compared to the oxide reduction currents. The charge density is related to the geometric surface area deduced from the as-prepared electrodes, and it is a measure of the oxide thickness, which will be discussed in more detail elsewhere.

Roughness factor - RF: For all materials, we determined the increase in surface area from the current in the double-layer region of the CVs recorded at a scan rate of 50 mV s^{-1} before and after electrolysis. This ratio is denoted as roughness factor (RF). The evaluation was performed on CVs where neither Faraday reactions nor adsorption processes occur before and after the electrolysis (or electrochemical reduction).[53] The respective potentials from which the RF was determined are 0.87 V for Au, 0.50 V for Pt, and -0.24 V for Cu. The last recorded CV before the electrolysis contained the information on the RF before the electrolysis. Direct information on the RF of Au and Cu after the electrolysis is not accessible since the oxide reduction currents strongly overlap with the double layer region in the CV. Therefore we determined the RF after the electrolysis from the last CV recorded after the complete reduction of the surface. Note that strictly speaking, this approach reveals the increase in electrochemical active surface area. Also, since the RF describes a ratio between the initial and final roughness, information on the absolute surface roughness cannot be determined with this approach.

Structural characterization: The morphology and microscopic structural properties of the wires were investigated using a Quattro S scanning electron microscope (SEM) from Thermo Scientific operating at an acceleration voltage of 10 or 20 kV. The optical microscope images were taken with the Leica S9i.

Acknowledgment

This work was supported by the Deutsche Forschungsgemeinschaft (DFG) through Grant No. SFB-CRC1316 (collaborative research center). EA would like to thank the "Stiftung Stipendien-Fonds des Verbandes der Chemischen Industrie (VCI)" for the financial support provided by a Kekulé scholarship.

CRediT

E. Artmann: Conceptualization, Formal Analysis, Funding Acquisition, Investigation, Validation, Visualization, Writing - Original Draft Preparation. **P. V. Menezes**: Investigation, Writing - Review & Editing. **L. Forschner**: Investigation, Writing - Review & Editing. **M. M. Elnagar**: Investigation, Writing - Review & Editing. **L. A. Kibler**: Writing - Review & Editing. **T. Jacob**: Funding Acquisition, Resources, Supervision, Writing - Review & Editing. **A. K. Engstfeld**: Conceptualization, Supervision, Writing - Review & Editing

Keywords

Contact Glow Discharge Electrolysis, Electrode stability, Platinum, Gold; Copper, Electrolysis

References

(1) Yerokhin, A.; Mukaeva, V. R.; Parfenov, E. V.; Laugel, N.; Matthews, A. Charge transfer mechanisms underlying Contact Glow Discharge Electrolysis. *Electrochimica Acta* **2019**, *312*, 441–456.

(2) Uosaki, K. *Electrochemical Science for a Sustainable Society: A Tribute to John O'M Bockris*; Springer, 2017.

(3) Schmickler, W.; Santos, E. *Interfacial electrochemistry*; Springer Science & Business Media, 2010.

(4) Yang, G.; Wang, B.; Tawfiq, K.; Wei, H.; Zhou, S.; Chen, G. Electropolishing of surfaces: theory and applications. *Surface Engineering* **2017**, *33*, 149–166.

(5) Bruggeman, P. J. et al. Plasma–liquid interactions: a review and roadmap. *Plasma Sources Science and Technology* **2016**, *25*, 053002.

(6) Belkin, P. N.; Kusmanov, S. A.; Parfenov, E. V. Mechanism and technological opportunity of plasma electrolytic polishing of metals and alloys surfaces. *Applied Surface Science Advances* **2020**, *1*, 100016.

(7) Horikoshi, S.; Serpone, N. In-liquid plasma: a novel tool in the fabrication of nanomaterials and in the treatment of wastewaters. *RSC Adv* **2017**, *7*, 47196–47218.

(8) Yanson, A. I.; Rodriguez, P.; Garcia-Araez, N.; Mom, R. V.; Tichelaar, F. D.; Koper, M. T. M. Cathodic corrosion: a quick, clean, and versatile method for the synthesis of metallic nanoparticles. *Angewandte Chemie (International ed. in English)* **2011**, *50*, 6346–6350.

(9) Saito, G.; Akiyama, T. Nanomaterial Synthesis Using Plasma Generation in Liquid. *J. Nanomater.* **2015**, *2015*, 1–21.

(10) Kellogg, H. H. Anode Effect in Aqueous Electrolysis. *Journal of The Electrochemical Society* **1950**, *97*, 133.

(11) Hickling, A and Ingram, MD, Contact glow-discharge electrolysis. *Transactions of the Faraday Society* **1964**, 783–793.

(12) Sen Gupta, S. K.; Singh, R. Cathodic contact glow discharge electrolysis: its origin and non-faradaic chemical effects. *Plasma Sources Science and Technology* **2017**, *26*, 015005.

(13) Jin, X.; Wang, X.; Yue, J.; Cai, Y.; Zhang, H. The effect of electrolyte constituents on contact glow discharge electrolysis. *Electrochimica Acta* **2010**, *56*, 925–928.

(14) Azumi, K.; Mizuno, T.; Akimoto, T.; Ohmori, T. Light Emission from Pt during High–Voltage Cathodic Polarization. *Journal of The Electrochemical Society* **1999**, *146*, 3374–3377.

(15) Yerokhin, A. L.; Nie, X.; Leyland, A.; Matthews, A.; Dowey, S. J. Plasma electrolysis for surface engineering. *Surface and Coatings Technology* **1999**, *122*, 73–93.

(16) Sengupta, S. K.; Singh, O. P. Contact glow discharge electrolysis: a study of its onset and location. *Journal of Electroanalytical Chemistry and Interfacial Electrochemistry* **1991**, *301*, 189–197.

(17) Sengupta, S. K.; Singh, O. P. Contact glow discharge electrolysis: a study of its chemical yields in aqueous inert-type electrolytes. *J. Electroanal. Chem.* **1994**, *369*, 113–120.

(18) Zheng, B.; Wang, K.; Shrestha, M.; Schuelke, T.; Fan, Q. H. Understanding the chemical reactions in cathodic plasma electrolysis. *Plasma Sources Science and Technology* **2019**, *28*, 085016.

(19) Landolt, D. Fundamental aspects of electropolishing. *Electrochimica Acta* **1987**, *32*, 1–11.

(20) Arulmozhi, N.; Hersbach, T. J. P.; Koper, M. T. M. Nanoscale morphological evolution of monocrystalline Pt surfaces during cathodic corrosion. *Proceedings of the National Academy of Sciences of the United States of America* **2020**, *117*, 32267–32277.

(21) Elnagar, M. M.; Hermann, J. M.; Jacob, T.; Kibler, L. A. An affordable option to Au single crystals through cathodic corrosion of a wire: Fabrication, electrochemical behavior, and applications in electrocatalysis and spectroscopy. *Electrochimica Acta* **2021**, *372*, 137867.

(22) Elnagar, M. M.; Hermann, J. M.; Jacob, T.; Kibler, L. A. Tailoring the electrode surface structure by cathodic corrosion in alkali metal hydroxide solution: Nanostructuring and faceting of Au. *Current Opinion in Electrochemistry* **2021**, *27*, 100696.

(23) Sen Gupta, S. K. Contact Glow Discharge Electrolysis: A Novel Tool for Manifold Applications. *Plasma Chem. Plasma Process* **2017**, *37*, 897–945.

(24) Clyne, T. W.; Troughton, S. C. A review of recent work on discharge characteristics during plasma electrolytic oxidation of various metals. *International Materials Reviews* **2019**, *64*, 127–162.

(25) Lu, X.; Mohedano, M.; Blawert, C.; Matykina, E.; Arrabal, R.; Kainer, K. U.; Zheludkevich, M. L. Plasma electrolytic oxidation coatings with particle additions – A review. *Surface and Coatings Technology* **2016**, *307*, 1165–1182.

(26) Barati Darband, G.; Aliofkhazraei, M.; Hamghalam, P.; Valizade, N. Plasma electrolytic oxidation of magnesium and its alloys: Mechanism, properties and applications. *Journal of Magnesium and Alloys* **2017**, *5*, 74–132.

(27) Nestler, K.; Böttger-Hiller, F.; Adamitzki, W.; Glowa, G.; Zeidler, H.; Schubert, A. Plasma Electrolytic Polishing – An Overview of Applied Technologies and Current Challenges to Extend the Polishable Material Range. *Procedia CIRP* **2016**, *42*, 503–507.

(28) Kareem, T. A.; Kaliani, A. A. Glow discharge plasma electrolysis for nanoparticles synthesis. *Ionics* **2012**, *18*, 315–327.

(29) Allagui, A.; Said, Z.; Abdelkareem, M. A.; Elwakil, A. S.; Yang, M.; Alawadhi, H. DC and AC Performance of Graphite Films Supercapacitors Prepared by Contact Glow Discharge Electrolysis. *Journal of The Electrochemical Society* **2017**, *164*, A2539–A2546.

(30) Allagui, A.; Baranova, E. A.; Wüthrich, R. Synthesis of Ni and Pt nanomaterials by cathodic contact glow discharge electrolysis in acidic and alkaline media. *Electrochimica Acta* **2013**, *93*, 137–142.

(31) Toriyabe, Y.; Watanabe, S.; Yatsu, S.; Shibayama, T.; Mizuno, T. Controlled formation of metallic nanoballs during plasma electrolysis. *Applied Physics Letters* **2007**, *91*, 041501.

(32) Saito, G.; Nakasugi, Y.; Yamashita, T.; Akiyama, T. Solution plasma synthesis of bimetallic nanoparticles. *Nanotechnology* **2014**, *25*, 135603.

(33) Kurniawan, F.; Rahmi, R. Synthesis of SnO_2 Nanoparticles by High Potential Electrolysis. *Bulletin of Chemical Reaction Engineering & Catalysis* **2017**, *12*, 281.

(34) Chen, Q.; Li, J.; Li, Y. A review of plasma–liquid interactions for nanomaterial synthesis. *Journal of Physics D: Applied Physics* **2015**, *48*, 424005.

(35) Malik, M. A.; Ghaffar, A.; Malik, S. A. Water purification by electrical discharges. *Plasma Sources Science and Technology* **2001**, *10*, 82–91.

(36) Wang, X.; Zhou, M.; Jin, X. Application of glow discharge plasma for wastewater treatment. *Electrochim. Acta* **2012**, *83*, 501–512.

(37) Gao, J.; Wang, X.; Hu, Z.; Deng, H.; Hou, J.; Lu, X.; Kang, J. Plasma degradation of dyes in water with contact glow discharge electrolysis. *Water Research* **2003**, *37*, 267–272.

(38) Pettersson, J.; Ramsey, B.; Harrison, D. A review of the latest developments in electrodes for unitised regenerative polymer electrolyte fuel cells. *Journal of Power Sources* **2006**, *157*, 28–34.

(39) Antolini, E. Review in Applied Electrochemistry. Number 54 Recent Developments in Polymer Electrolyte Fuel Cell Electrodes. *Journal of Applied Electrochemistry* **2004**, *34*, 563–576.

(40) Noerskov, J. K.; Bligaard, T.; Logadottir, A.; Kitchin, J. R.; Chen, J. G.; Pandelov, S.; Stimming, U. Trends in the Exchange Current for Hydrogen Evolution. *ChemInform* **2005**, *36*.

(41) Climent, V.; Feliu, J. M. Thirty years of platinum single crystal electrochemistry. *J. Solid State Electrochem.* **2011**, *15*, 1297–1315.

(42) Trasatti, S. Work function, electronegativity, and electrochemical behaviour of metals. *Journal of Electroanalytical Chemistry and Interfacial Electrochemistry* **1972**, *39*, 163–184.

(43) Hammer, B.; Norskov, J. K. Why gold is the noblest of all the metals. *Nature* **1995**, *376*, 238–240.

(44) Burke, L. D. Scope for new applications for gold arising from the electrocatalytic behaviour of its metastable surface states. *Gold Bulletin* **2004**, *37*, 125–135.

(45) Tremiliosi-Filho, G.; Dall'Antonia, L. H.; Jerkiewicz, G. Limit to extent of formation of the quasi-two-dimensional oxide state on Au electrodes. *Journal of Electroanalytical Chemistry* **1997**, *422*, 149–159.

(46) Hori, Y. Electrochemical CO2 Reduction on Metal Electrodes. *42*, 89–189.

(47) Gao, D.; Zegkinoglou, I.; Divins, N. J.; Scholten, F.; Sinev, I.; Grosse, P.; Roldan Cuenya, B. Plasma-Activated Copper Nanocube Catalysts for Efficient Carbon Dioxide Electroreduction to Hydrocarbons and Alcohols. *ACS nano* **2017**, *11*, 4825–4831.

(48) Nitopi, S.; Bertheussen, E.; Scott, S. B.; Liu, X.; Engstfeld, A. K.; Horch, S.; Seger, B.; Stephens, I. E. L.; Chan, K.; Hahn, C.; Nørskov, J. K.; Jaramillo, T. F.; Chorkendorff, I. Progress and Perspectives of Electrochemical CO2 Reduction on Copper in Aqueous Electrolyte. *Chemical reviews* **2019**, *119*, 7610–7672.

(49) Yatsu, S.; Takahashi, H.; Sasaki, H.; Sakaguchi, N.; Ohkubo, K.; Muramoto, T.; Watanabe, S. Fabrication of nanoparticles by electric discharge plasma in liquid. *Archives of Metallurgy and Materials* **2013**,

(50) Akolkar, R.; Sankaran, R. M. Charge transfer processes at the interface between plasmas and liquids. *Journal of Vacuum Science & Technology A: Vacuum, Surfaces, and Films* **2013**, *31*, 050811.

(51) Mandin, P.; Wüthrich, R.; Roustan, H. Polarization curves for an alkaline water electrolysis at a small pin vertical electrode to produce hydrogen. *AIChE Journal* **2010**, *33*, 2446–2454.

(52) Kibler, L. A. Preparation and characterization of noble metal single crystal electrode surfaces. *International Society of Electrochemistry* **2003**, 1–55.

(53) Łukaszewski, M. Electrochemical Methods of Real Surface Area Determination of Noble Metal Electrodes – an Overview. *International Journal of Electrochemical Science* **2016**, 4442–4469.

(54) Daubinger, P.; Kieninger, J.; Unmüssig, T.; Urban, G. A. Electrochemical characteristics of nanostructured platinum electrodes–a cyclic voltammetry study. *Physical chemistry chemical physics : PCCP* **2014**, *16*, 8392–8399.

(55) Itaya, K.; Sugawara, S.; Sashikata, K.; Furuya, N. Insitu scanning tunneling microscopy of platinum (111) surface with the observation of monatomic steps. *Journal of Vacuum Science & Technology A: Vacuum, Surfaces, and Films* **1990**, *8*, 515–519.

(56) Arulmozhi, N.; Esau, D.; Lamsal, R. P.; Beauchemin, D.; Jerkiewicz, G. Structural Transformation of Monocrystalline Platinum Electrodes upon Electro-oxidation and Electro-dissolution. *ACS Catalysis* **2018**, *8*, 6426–6439.

(57) Jacobse, L.; Huang, Y.-F.; Koper, M. T. M.; Rost, M. J. Correlation of surface site formation to nanoisland growth in the electrochemical roughening of Pt(111). *Nature materials* **2018**, *17*, 277–282.

(58) Fuchs, T.; Drnec, J.; Calle-Vallejo, F.; Stubb, N.; Sandbeck, D. J. S.; Ruge, M.; Cherevko, S.; Harrington, D. A.; Magnussen, O. M. Structure dependency of the atomic-scale mechanisms of platinum electro-oxidation and dissolution. *Nature Catalysis* **2020**, *3*, 754–761.

(59) Sengupta, S. K. A Study on the Origin of Nonfaradaic Behavior of Anodic Contact Glow Discharge Electrolysis. *Journal of The Electrochemical Society* **1998**, *145*, 2209.

(60) Jin, X.-L.; Wang, X.-Y.; Zhang, H.-M.; Xia, Q.; Wei, D.-B.; Yue, J.-J. Influence of Solution Conductivity on Contact Glow Discharge Electrolysis. *Plasma Chemistry and Plasma Processing* **2010**, *30*, 429–436.

(61) Gangal, U.; Srivastava, M.; Sen Gupta, S. K. Mechanism of the Breakdown of Normal Electrolysis and the Transition to Contact Glow Discharge Electrolysis. *Journal of The Electrochemical Society* **2009**, *156*, F131.

(62) Kirchhoff, B.; Braunwarth, L.; Jung, C.; Jónsson, H.; Fantauzzi, D.; Jacob, T. Simulations of the Oxidation and Degradation of Platinum Electrocatalysts. *Small (Weinheim an der Bergstrasse, Germany)* **2020**, *16*, e1905159.

(63) Sukeri, A.; Bertotti, M. Nanoporous Gold Surface: An Efficient Platform for Hydrogen Evolution Reaction at Very Low Overpotential. *Journal of the Brazilian Chemical Society* **2017**,

(64) Vitrey, A.; Alvarez, R.; Palmero, A.; González, M. U.; García-Martín, J. M. Fabrication of black-gold coatings by glancing angle deposition with sputtering. *Beilstein journal of nanotechnology* **2017**, *8*, 434–439.

(65) Zheng, H.; Picard, C.; Ravaine, S. Nanostructured gold films exhibiting almost complete absorption of light at visible wavelengths. *Frontiers of Chemical Science and Engineering* **2018**, *12*, 247–251.

(66) Vvedenskii, A.; Grushevskaya, S.; Ganzha, S.; Eliseev, D. Copper oxides: kinetics of formation and semiconducting properties. Part I. Polycrystalline copper and copper-gold alloys. *Journal of Solid State Electrochemistry* **2014**, *18*, 2755–2770.

(67) Vvedenskii, A.; Grushevskaya, S.; Ganzha, S.; Eliseev, D.; Abakumova, L. I. Copper oxides: kinetics of formation and semiconducting properties. Part II. Copper single crystals. *Journal of Solid State Electrochemistry* **2014**, *18*, 3437–3451.

(68) Deng, Y.; Handoko, A. D.; Du, Y.; Xi, S.; Yeo, B. S. In Situ Raman Spectroscopy of Copper and Copper Oxide Surfaces during Electrochemical Oxygen Evolution Reaction: Identification of Cu III Oxides as Catalytically Active Species. *ACS Catalysis* **2016**, *6*, 2473–2481.

(69) Engstfeld, A. K.; Maagaard, T.; Horch, S.; Chorkendorff, I.; Stephens, I. E. L. Polycrystalline and Single-Crystal Cu Electrodes: Influence of Experimental Conditions on the Electrochemical Properties in Alkaline Media. *Chemistry (Weinheim an der Bergstrasse, Germany)* **2018**, *24*, 17743–17755.

(70) P. Schouten, K. J.; Gallent, E. P.; Koper, M. T. The electrochemical characterization of copper single-crystal electrodes in alkaline media. *Journal of Electroanalytical Chemistry* **2013**, *699*, 6–9.

(71) Bagger, A.; Arán-Ais, R. M.; Halldin Stenlid, J.; Campos Dos Santos, E.; Arnarson, L.; Degn Jensen, K.; Escudero-Escribano, M.; Roldan Cuenya, B.; Rossmeisl, J. Ab Initio Cyclic Voltammetry on Cu(111), Cu(100) and Cu(110) in Acidic, Neutral and Alkaline Solutions. *Chemphyschem : a European journal of chemical physics and physical chemistry* **2019**, *20*, 3096–3105.

(72) Tiwari, A.; Heenen, H. H.; Bjørnlund, A. S.; Maagaard, T.; Cho, E.; Chorkendorff, I.; Kristoffersen, H. H.; Chan, K.; Horch, S. Fingerprint Voltammograms of Copper Single Crystals under Alkaline Conditions: A Fundamental Mechanistic Analysis. *The journal of physical chemistry letters* **2020**, *11*, 1450–1455.

SUPPORTING INFORMATION -

Structural evolution of Pt, Au, and Cu anodes by electrolysis up to contact glow discharge electrolysis in alkaline electrolytes

Evelyn Artmann, Vincent P. Menezes, Lukas Forschner, Mohamed M. Elnagar, Ludwig A. Kibler, Timo Jacob,* and Albert K. Engstfeld*

Institute of Electrochemistry, Ulm University, D-89081 Ulm, Germany

E-mail: timo.jacob@uni-ulm.de; albert.engstfeld@uni-ulm.de

Phone: +49 (0)731 25401. Fax: +49 (0)731 25409

S1: Temperature effects on the I–U characteristics

Figure S1 shows the chronoamperometric curves obtained for electrolysis on Pt in 0.01 M KOH for 30 s at the indicated voltages, where in a) the the applied voltage and in b) the resulting current is plotted *vs.* time. Overall, the applied voltages are very stable. The currents are also nearly constant when low voltages are applied to the electrode (up to 300 V). At about 300 V, the current increases slowly with time. At voltages higher than 300 V, the current density increases slowly at first (NE region). After some time, the current density breaks down, marking the moment when the plasma in solution is ignited.

The phenomena observed in the I–t behavior can be explained by the increase in electrolyte temperature due to Joule heating, which is more pronounced for higher voltages and current densities.[1,2] In the NE region the increase in current density is explained by the increase in conductivity of the 0.01 M KOH solution with increase temperature.[3] When the voltage is high enough and the temperature of the electrolyte near the electrode reaches a certain value, the current density breaks down. Therefore the breakdown occurs earlier for the higher voltages where Joule heating is more pronounced.

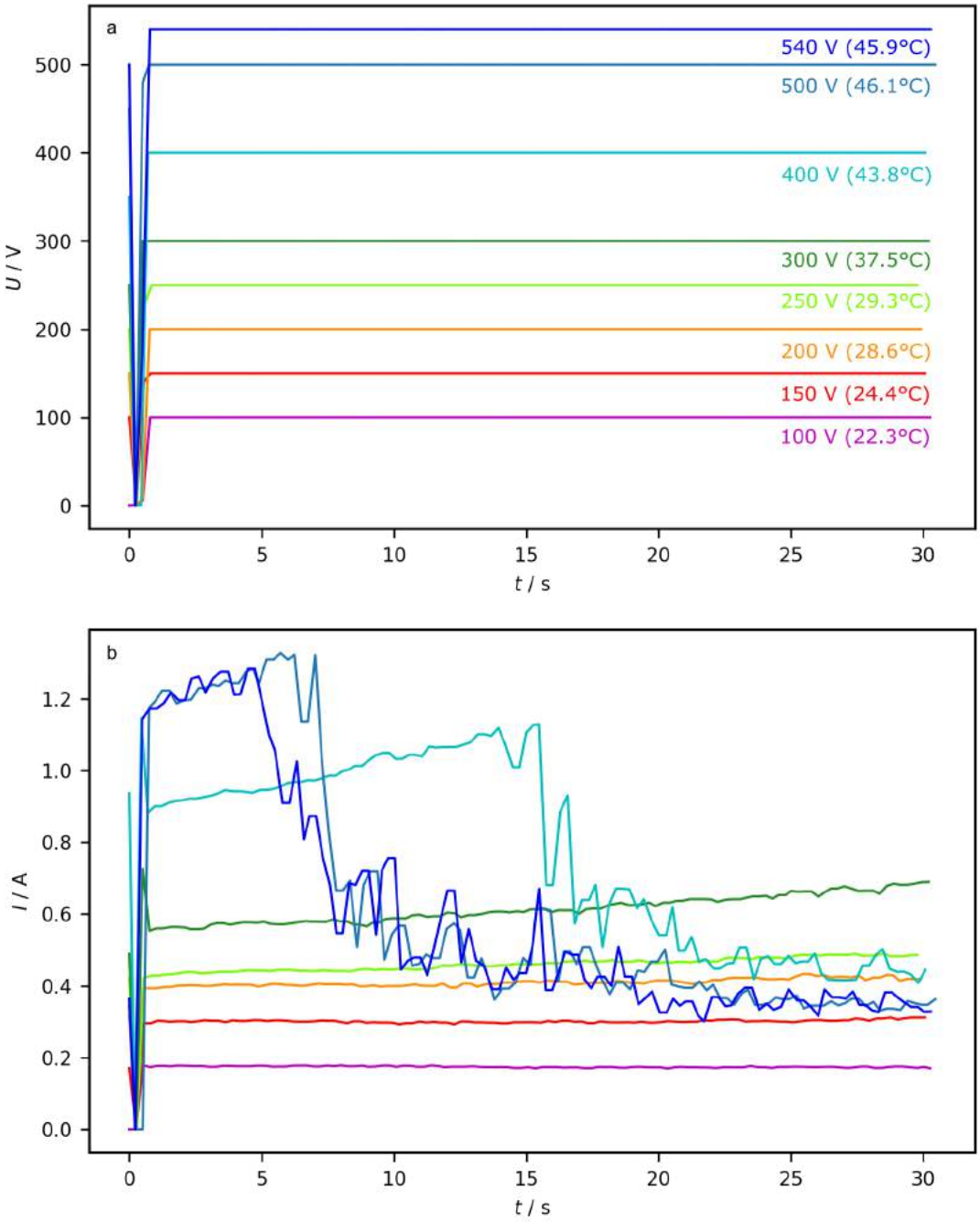

Figure S1: Chronoamperometry of a Pt wire electrode for 30 s in 0.01 M KOH at different voltages. The temperature in the brackets after the respective voltage is the temperature after electrolysis. a) applied voltages vs. time. b) Evolution of the current densities at the given voltages. Each measurement was performed with a freshly prepared wire and new electrolyte.

The individual values in the *I–U* plot of Fig. 1 a) in the manuscript are obtained by averaging the current density values in Fig. S1 b) over the entire 30 s of electrolysis (see experimental section). Typically the *I-–U* characteristics are studied by varying the applied voltage linearly with a specific constant scan rate (linear sweep voltammetry – LSV).[2,4,5] To mimic this situation, we also studied the electrodes by staircase voltammetry (SCV). The voltage was then increased from 20 V every 10 s in 20 V steps until the desired final voltage of 540 V was reached. A comparison between the stationary *I–U* curve from Fig. 1 (blue dashed line) in the manuscript and the resulting SCV *I–U* curve (red solid line) is shown in Fig- S2. In the SCV plot, the individual points are average current density values recorded at the specific voltages.

Comparing both experimental approaches, the temperature effect does not play a significant role in the NE region (on the time scales of the experiment) since the curves are almost identical. The breakdown voltage of the electrolyte occurs at lower voltages in the SCV measurement. This can be rationalized by a higher electrolyte temperature, explained as follows. As already shown in Fig. S1, the increase of the electrolyte temperature near the electrode becomes significant at around 300 V. Furthermore, in the SCV experiment the electrolyte is continuously heated already before reaching 300 V, which presumably leads to overall higher electrolyte temperatures already at around 300 V, not only near the electrode. The effect of the different electrolyte temperatures in both experiments becomes apparent at high voltages, where at 540 V the temperature of the electrolyte after the SCV experiment is almost 40 K higher than in the chronoamperometry experiment. The difference in electrolyte temperature has an effect on the current density, which is lower in the SCV experiment than in the stationary current experiment. One explanation is that the higher electrolyte temperature makes it easier to bring the electrolyte near the electrode to the boiling point. This in turn means that less power is required to discharge the gas between the electrode and the electrolyte.[1,5–7]

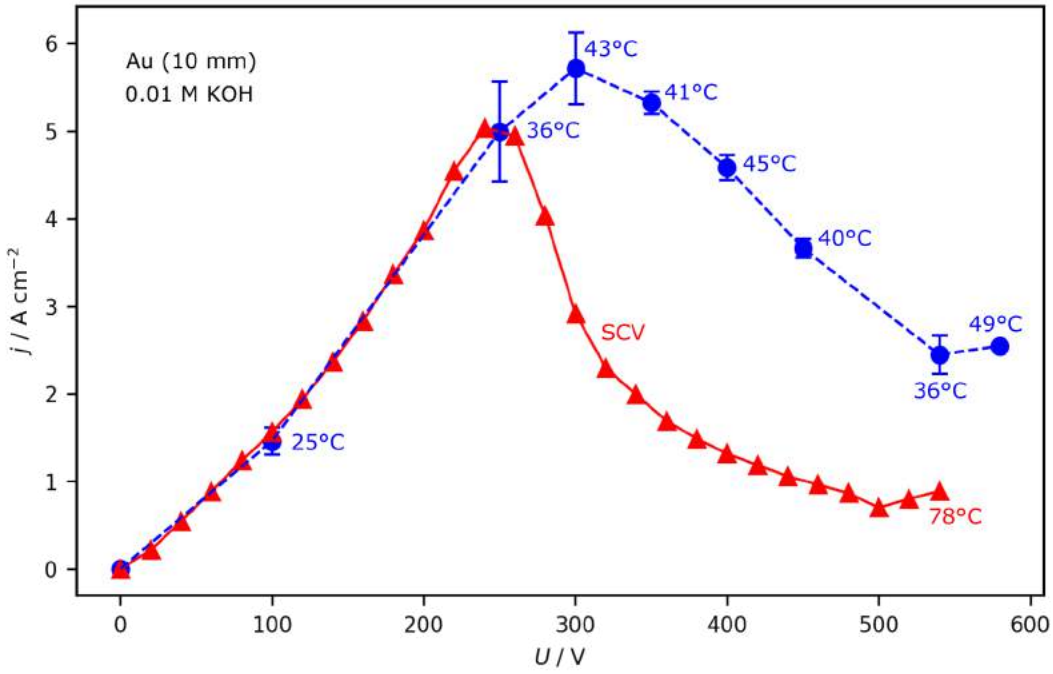

Figure S2: SCV recorded on a Au wire electrode in 0.01 M KOH between 0 and 560 V (20 V steps every 10 s) (red solid line) and stationary I-U curve from Fig. 1 a in the manuscript (blue dashed line and circles). The temperatures given next to the data points are the electrolyte temperatures recorded after the respective electrolysis experiments.

S2: SEM Pt

Figure S3 shows SEM images of an as-prepared Pt electrode in a) as well as after 30 s electrolysis at 100, 300 and 580 V in b) to d). As already mentioned in the manuscript itself, no significant restructuring of the Pt electrode is observed after the electrolysis for all investigated electrolysis voltages.

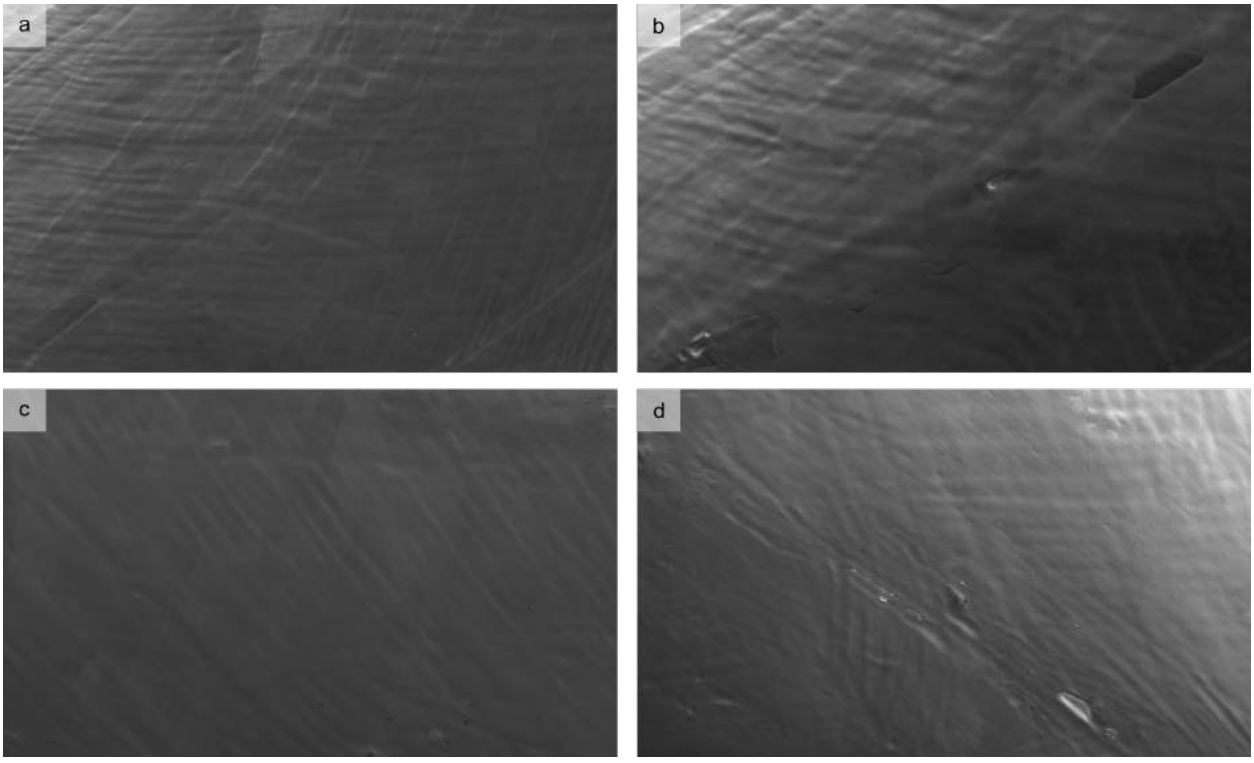

Figure S3: SEM images (250 µm × 150 µm) of a Pt wire electrode a) as-prepared and after electrolysis in 0.01 M KOH for 30 s at b) 100 V, c) 300 V and d) 580 V.

S3: SEM Au

S3.1: Beam Damage

Figure S4 demonstrates the effect of electron beam damage during SEM on the Au_2O_3 structures formed by electrolysis at 300 V for 30 s in 0.01 M KOH and direct removal of the electrode from the electrolyte. In the SEM images taken successively at the same location in a) and b), the increase in number and formation of holes in the oxide layer can be seen. Also, when zooming out in c), the area scanned in a) and b) appears much brighter, indicating that the electronic structure of the electrode in this area changed.

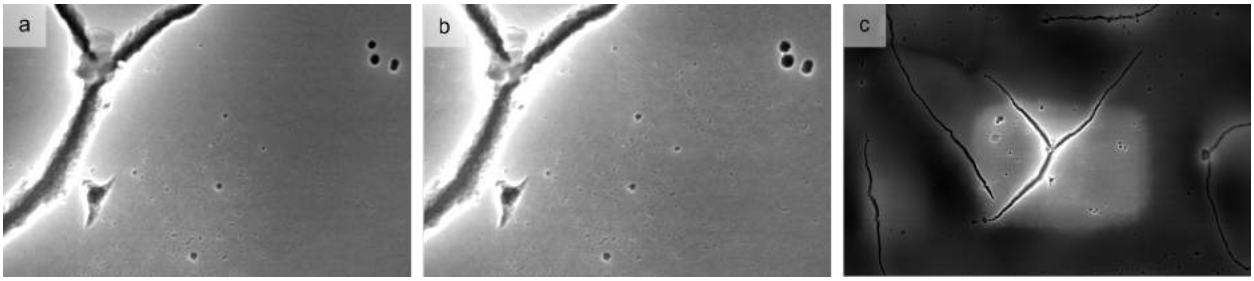

Figure S4: SEM image sequence of a particular spot of a Au wire after electrolysis at 300 V for 30 s in 0.01 M KOH and direct removal of the electrode from the electrolyte. Where a) and b) show images measured consecutively at the same location with identical image sizes and c) shows the next image after zoom out from the region depicted in a) and b). SEM image sizes are in a) and b) 6 µm × 4 µm and c) 24 µm × 16 µm.

S3.2:Electrode structure after electrolysis and electrochemical reduction

Figure S5 a) shows an SEM image of a Au electrode after electrolysis at 300 V for 30 s and direct removal from the electrolysis solution. The surface consists of a solid Au_2O_3 film with cracks, as described in the manuscript. Figure S5 b) shows an SEM image of the same electrode but after electrochemical reduction (see main text for details). The formerly solid Au_2O_3 film transformed into a porous structure similar in appearance to that obtained by holding the electrode after the electrolysis for 60 s in the electrolysis solution, shown in Fig. 5 m) to p) in the manuscript. A more detailed description of the Au_2O_3 formation during electrolysis, the the porous Au film formation during the subsequent reduction as well as the role of H_2O_2 in the reduction of the Au_2O_3 film, is given elsewhere.

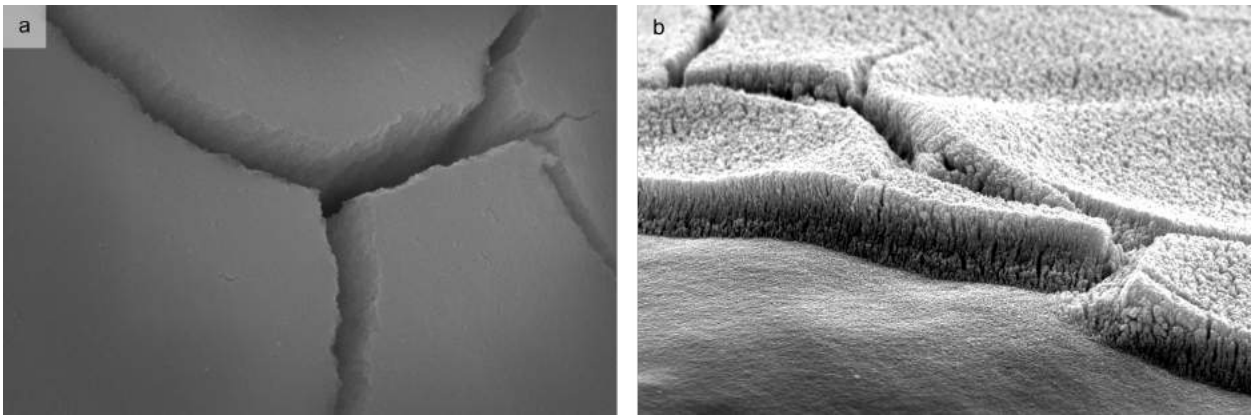

Figure S5: SEM images (6 µm × 4 µm) of a Au wire electrode a) after electrolysis at 300 V for 30 s in 0.01 M KOH and direct removal of the electrode from the electrolysis solution and b) the same electrode after electrochemical reduction.

S4: SEM Cu

S4.1: Large area SEM images of Cu electrodes after electrolysis

From the SEM images in Fig. S6 taken on Cu electrodes removed immediately after the electrolysis and those left in the electrolysis solution, no clear differences in the structural properties can be seen.

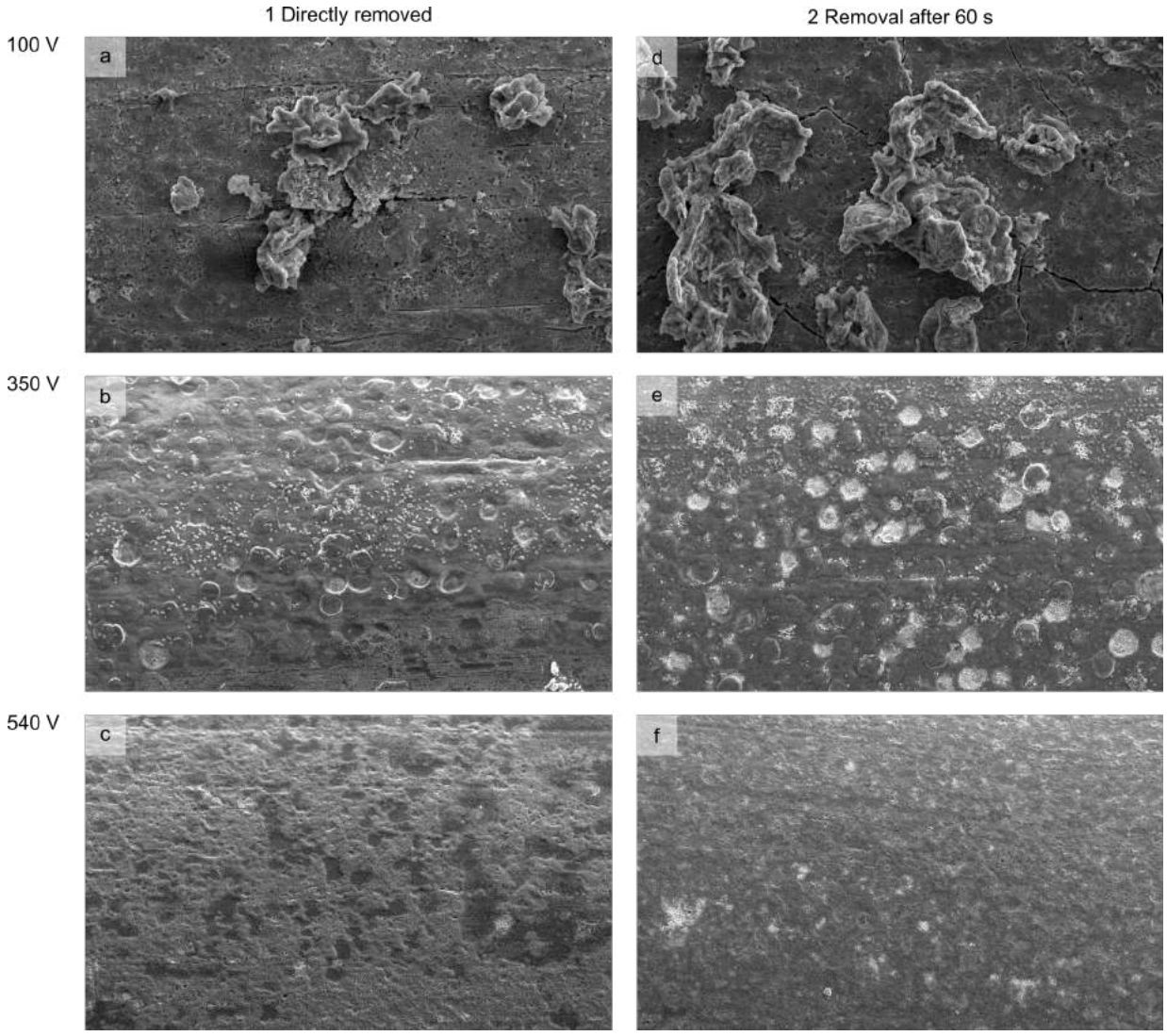

Figure S6: SEM images (250 µm × 150 µm) of Cu wire electrodes after electrolysis for 30 s in 0.01 M KOH at the voltages given in each row. The first column (a) to c)) shows the surface after direct removal of the electrodes from the electrolysis solution. The second column (d) to f)) shows electrodes which were treated in the same way but which were kept for additional 60 s in the electrolysis solution.

S4.2: Electrode structure after electrolysis and electrochemical reduction

Fig. S7 demonstrates that Cu oxides formed by electrolysis turn into a porous film after electrochemical reduction. The effect is shown for an electrode which was removed immediately after the electrolysis and another electrode that was kept in the electrolysis solution for 60 s.

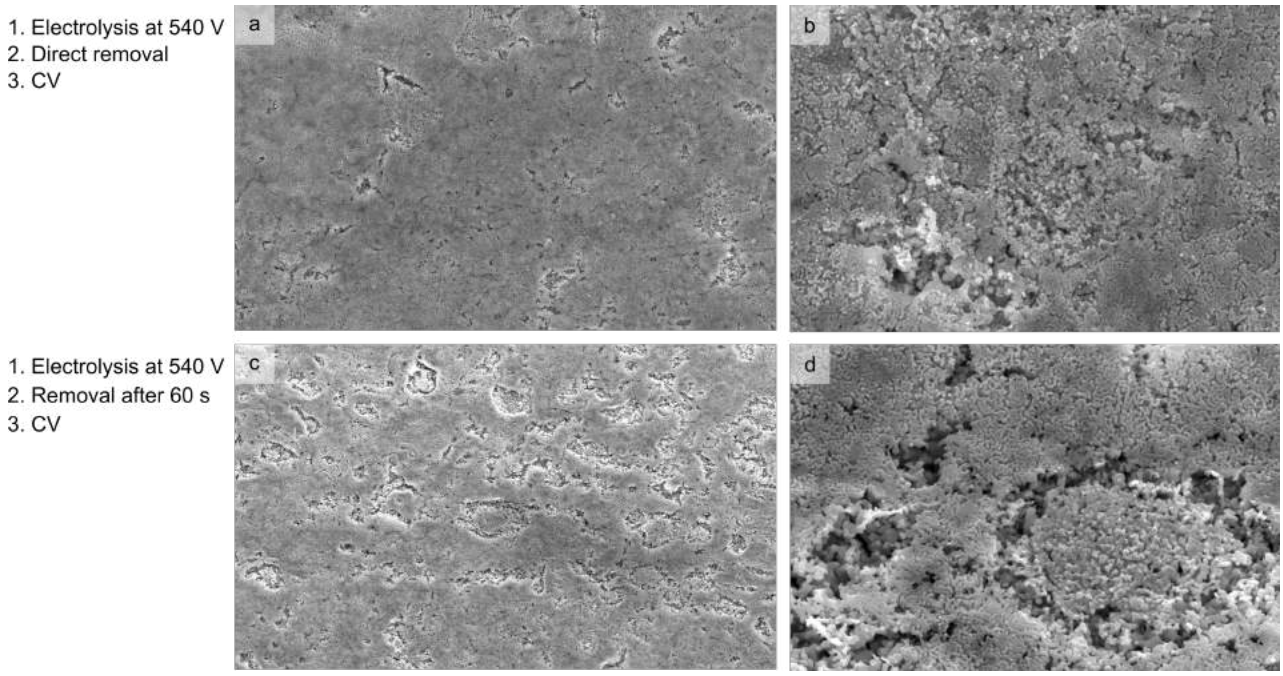

Figure S7: SEM images of Cu wire electrodes after electrolysis at 540 V for 30 s in 0.01 M KOH and subsequent electrochemical reduction. a) and b) show electrodes which were reduced electrochemically directly after removing the electrodes from the electrolysis solution. In c) and d) the electrodes were reduced after keeping the electrode for additional 60 s in the electrolysis solution. b) and d) are enlargement views of the structures in the images a) and c), respectively. Image size in a) and c) 50 µm × 30 µm and in b) and d) 6 µm × 4 µm

References

(1) Yerokhin, A.; Mukaeva, V. R.; Parfenov, E. V.; Laugel, N.; Matthews, A. Charge transfer mechanisms underlying Contact Glow Discharge Electrolysis. *Electrochimica Acta* **2019**, *312*, 441–456.

(2) Azumi, K.; Mizuno, T.; Akimoto, T.; Ohmori, T. Light Emission from Pt during High–Voltage Cathodic Polarization. *Journal of The Electrochemical Society* **1999**, *146*, 3374–3377.

(3) Gilliam, R.; Graydon, J.; Kirk, D.; Thorpe, S. A review of specific conductivities of potassium hydroxide solutions for various concentrations and temperatures. *International Journal of Hydrogen Energy* **2007**, *32*, 359–364.

(4) Saito, G.; Nakasugi, Y.; Akiyama, T. Generation of solution plasma over a large electrode surface area. *Journal of applied physics* **2015**, *118*, 023303.

(5) Mandin, P.; Wüthrich, R.; Roustan, H. Polarization curves for an alkaline water electrolysis at a small pin vertical electrode to produce hydrogen. *AIChE Journal* **2010**, *33*, 2446–2454.

(6) Kellogg, H. H. Anode Effect in Aqueous Electrolysis. *Journal of The Electrochemical Society* **1950**, *97*, 133.

(7) Hickling, A and Ingram, MD, Contact glow-discharge electrolysis. *Transactions of the Faraday Society* **1964**, 783–793.